INVESTIGATION OF THE SELENIUM TO METAL EVAPORATION RATIO WITH RESPECT TO ABSORBER STRUCTURE AND ELECTRICAL PROPERTIES OF CU(IN,GA)SE_2 THIN FILM SOLAR CELLS

Enrico Jarzembowski[a], Stefan Hartnauer[a], Wolfgang Fränzel[a], Kai Kaufmann[b], Roland Scheer[a]
[a]Martin-Luther-University Halle-Wittenberg, Institute of Physics, 06120 Halle, Germany
[b]Hochschule Anhalt, University of Applied Sciences, 06366 Köthen, Germany
Phone: +49-345-5525492, e-mail: enrico.jarzembowski@physik.uni-halle.de

ABSTRACT: In this work, a series of Mo/Cu(In,Ga)Se_2/CdS/ZnO solar cells was investigated, with absorber layers prepared by means of a three-stage co-evaporation process [1] with varying selenium flow (Se/Me=2-8) at two different first stage substrate temperatures (400°C, 490°C). The used methods to characterize the absorber material are EDX, XRD, ToF-SIMS and RAMAN measurements. We find that the preferred orientation of the CIGSe crystals changes from (112) to (220)/(204) if Se/Me is larger than four. Crystal size and RAMAN-spectral features are generally independent from the Se/Me-ratio. To determine the electrical properties we used I-V-measurements of completed solar cells. V_{OC}, J_{SC}, FF and η show a clear maximum at Se/Me=5.
Keywords: Cu(In,Ga)Se_2, Chalcopyrite, Thin Film Solar Cell

1 INTRODUCTION

The selenium to metal ratio (Se/Me) during Cu(In,Ga)Se_2 (CIGSe) deposition is a quantity of technological and electronic relevance. It has been reported that Se/Me can change the absorber growth [2-5], has impact on the cell efficiency [4-6], and may determine the metastable behavior of solar cells [7]. Certainly, a minimum Se/Me is favorable in terms of costs and equipment wear. The present work investigates the influence of the Selenium supply during absorber growth in a 3-stage process with a Gallium to Indium-Gallium (GGI) ratio of 0.37. To this end, we varied Se/Me between 2 and 8, which is calculated by dividing the Selenium flux through the Indium and Gallium fluxes, respectively the copper flux. The relatively high GGI aims at high V_{OC} devices being a general research direction. Our analysis shows a clear shift of the orientation from (112) to (220)/(204), with increasing Selenium pressure. Further, we observed an efficiency maximum at Se/Me=5. In comparison with our reference cell with GGI=0.24, this maximum is characterized by a slightly increased V_{OC}, but strongly decreased J_{SC}. We report on the Sodium profile in the structure and show an unusual maximum at the location of grain boundaries, measured by time of flight secondary ion mass spectroscopy (ToF-SIMS).

2 EXPERIMENTAL

The Cu(In,Ga)Se_2-absorber layers were prepared in a Balzers bak600 evaporation chamber. Our base pressure is $1.7 \cdot 10^{-7}$ mbar, realized by use of an oil diffusion pump and a cooling trap. For evaporation of the elements Cu, In, Ga, and Se, LUXEL Radak II furnaces were used. The substrate was heated by a graphite heater under constant rotation. The substrate temperature was measured with a thermocouple in contact with the back side of the substrate. We estimate that 625°C measured with the thermocouple is ~50 K higher than the real substrate temperature because we only slightly pass the glass transition temperature. The thickness of the Mo back contact is around 350-500 nm, with a sheet resistance of 0.65Ω/sq. Determination of the element fluxes was done with a quartz crystal microbalance (INFICON) at the substrate position. The element fluxes are: Indium 4.8Å/s, Gallium 1.7Å/s, Copper 3.7Å/s and Selenium 14-50Å/s. Hence we achieve the Se/Me-ratios: 7.7, 6.3, 5.0, 3.9 and 2.1 in the first and third stages and 13.5, 11.1, 8.8, 6.8 and 3.7 in the second stage. In the first stage, we used substrate temperatures of 400°C or 490°C up to a precursor thickness of ~1.6µm. At the beginning of the second stage, the substrate temperature was ramped up to 625°C and then held constant up to the end of the process. The Copper to Indium/Gallium ratio (CGI) at the end of stage 2 was 1.09 as calculated by use of laser light scattering (LLS) [8]. Then, the third stage started with the same In and Ga evaporation rates like in the first stage, but with higher substrate temperature. Finally, the substrate was cooled down to 350°C in 15 min under selenium atmosphere. Selenium rate is kept constant over the whole process. The total deposition time is in the range of 35-40 min and the final film thickness is 2.5-2.8 µm. The final CGI ratio was determined by energy dispersive x-ray spectroscopy (EDX) and is in the range of 0.87-0.98. The GGI was calculated from the external quantum efficiency (EQE). Our reference cell has GGI=0.24 and for the selenium variation we used GGI=0.33-0.37. The solar cells were completed with a ~50nm thick CdS layer, a ~500nm thick ZnO/ZnO:Al front contact and a Ni/Al-Grid. Finally we scribed the substrate into solar cells with an area of 0.5 cm^2.

3 RESULTS AND DISCUSSION

Figure 1 shows the X-ray diffraction patterns of the CIGSe-layers, prepared at $T_{Substrate}$=400°C in the first stage, under different Selenium pressure. The diffraction patterns for $T_{Substrate}$=490°C show the same behavior. A Se/Me-ratio equal or higher than 3.9 only leads to reflexes of the chalcopyrite structure, but with different orientation. Under the lowest Se/Me of 2.1, there is only the (112)-Peak of the chalcopyrite structure which is substantially shifted to larger angles. For this Se flux,

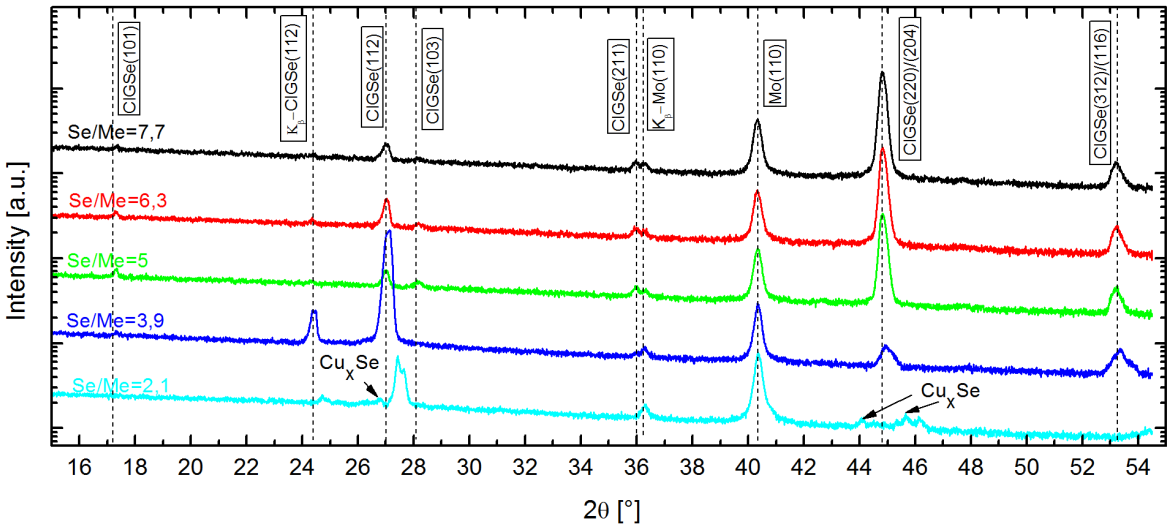

Figure 1: X-ray diffraction pattern for 400°C first stage temperature with different Se/Me-fluxes. The diffraction patterns for 490°C, show a similar behavior.

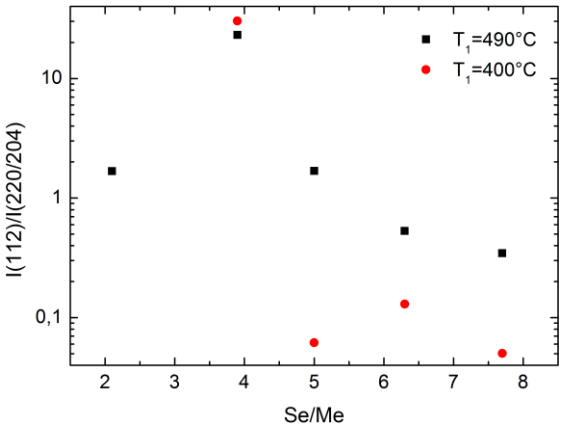

Figure 2: Intensity ratios $I_{(112)}/I_{(220)/(204)}$ versus Selenium to Metal fluxes.

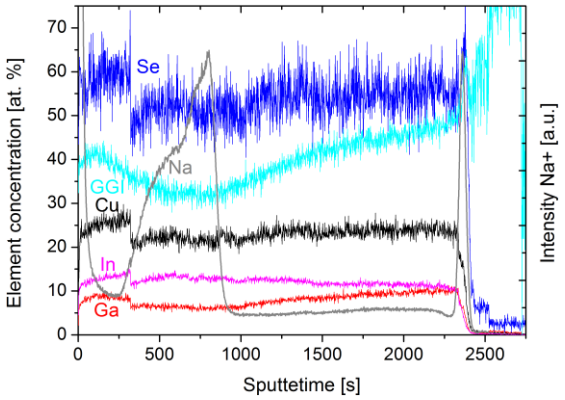

Figure 3: ToF-SIMS depth profile for 400°C first stage substrate temperature with Se/Me=7.7.

volatile In-Se compositions evaporate in the second process stage leading to the final formation of $CuGaSe_2$. Therefore the (112)-peaks are shifted to higher angles. This is in good agreement with the element composition, determined with EDX, which indicates the nearly absence of Indium. As all layers had the same thickness at the end of the first stage (determined by LLS), but the final film thickness of Se/Me=2.1 is <1µm, In-Se evaporation must take place in stages 2 and 3. The XRD-data show peaks that can be assigned to Cu_xSe which is in compliance with EDX-data (CGI>1.5). RAMAN measurements (not shown) show just CIGSe vibration modes at the same position, independent from Se/Me. Only for the lowest Se/Me-ratio we observed a shift towards larger RAMAN shifts, which corresponds to the higher Ga content. In order to investigate the grain orientation, the intensity area ratio between the (112)-peak and (220)/(204)-peak are plotted in figure 2. In general the orientation changes from (220)/(204) for high Se/Me-ratios up to highly (112) for lower Selenium pressures. This is in agreement with the findings in references [3–5]. Moreover the orientation depends on the first stage substrate temperature: Higher temperatures require higher Selenium pressure to yield (220)/(204)-orientation.

According to literature [5, 9] the preferred CIGSe orientation is based on the $(In,Ga)Se_2$-precursor orientation. Because of the higher Selenium desorption rate and the lower sticking coefficient, a higher Se/Me-ratio is needed at higher substrate temperatures in order to obtain the (220)/(204)-orientation. The following ToF-SIMS analysis (figure 3) shows the atomic percentage concentration of Cu, In, Ga, and Se and the distribution of Sodium inside the CIGSe layer of the sample with Se/Me=7.7 (T_1=400°C). A profile with Se/Me=5 does not exhibit fundamental differences. The GGI shows a V-shape gradient, which is typical for three-stage grown CIGSe absorber layers [10]. The Sodium concentration, however, shows a strong maximum at 1/3 layer thickness from the front contact. Due to the fact that Na is concentrated at grain boundaries, the Na-peak intensity suggests that at this position grain boundaries (GB) are located [11]. Hence a horizontal GB should exist over the whole absorber. Cross-section views by scanning electron microscopy confirm this fact (figure 4). At the bottom of the film large grains with low density of GBs can be seen while the top of the film is characterized by a horizontal GB and smaller grains. The GBs can act as recombination centers for the charge carriers and can lower the open circuit voltage and the fill factor. This is particularly the case if the grain boundaries are located

within the space charge region [12]. This type of grain structure exists in all samples, including the reference sample with GGI=0.24. Currently, we cannot explain the formation of this GB.

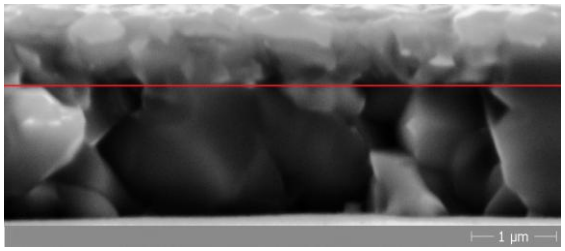

Figure 4: Cross-section view of the sample Se/Me=5 (400°C). The red line indicates the grain boundary at 1/3 film thickness.

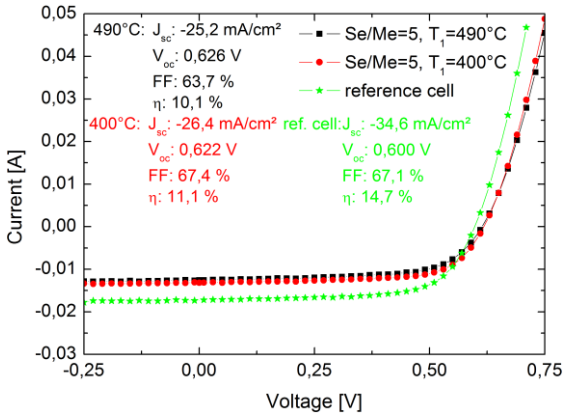

Figure 5: I-V curves from the best solar cells made from the Selenium variation in comparison to our reference solar cell.

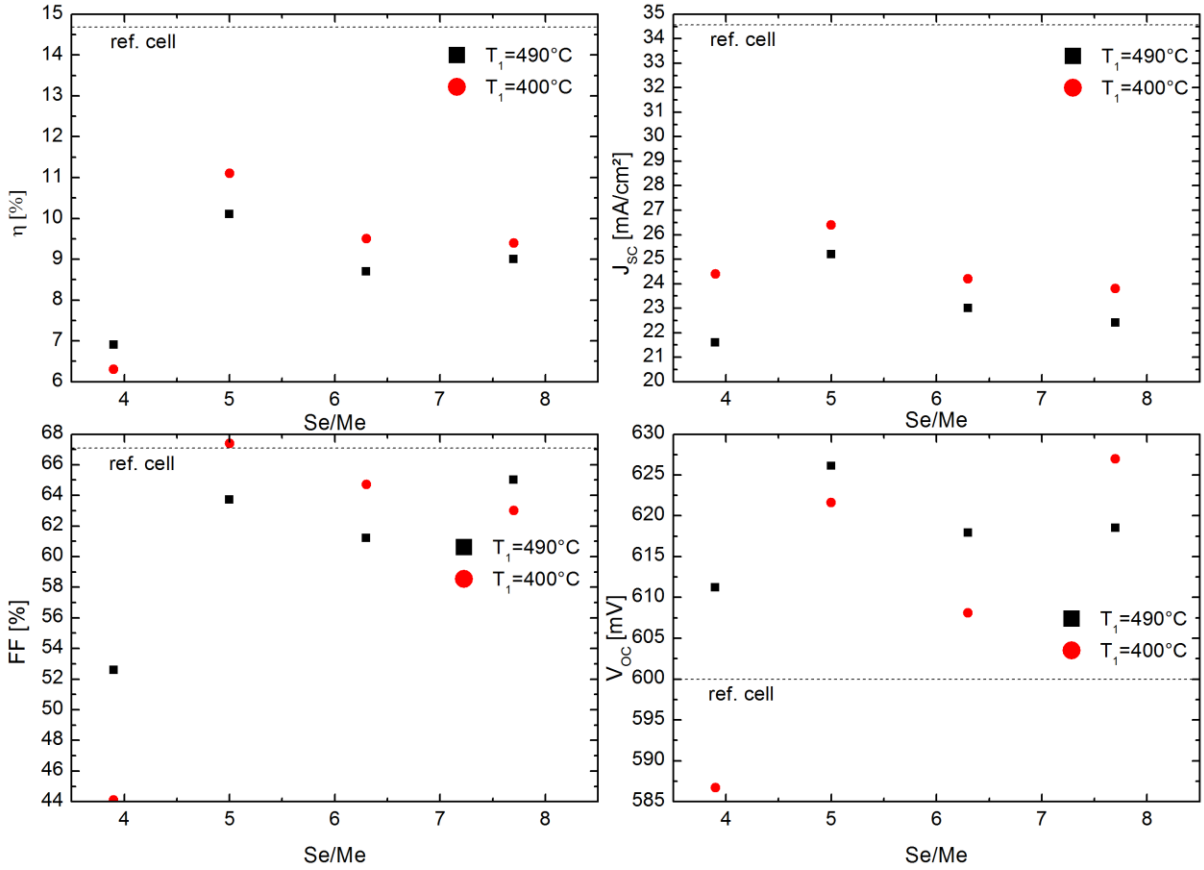

Figure 6: Solar cell parameters as a function of the Se/Me ratio. As comparison the parameters of the reference cell are represented by the dotted line.

The high Sodium concentration at the position of the horizontal GB is assumed to be the outcome of the GB [11]. At the same time the integral Na concentration may be the reason for the GB formation.

Figure 5 shows the I-V curves of the best solar cells from the selenium variation and the reference cell, under the illumination of 1000W/m^2. The best cells were prepared with Se/Me=5, in contrast to our reference cell with Se/Me=7. This is in disagreement with the literature where the solar cell parameters were found to increase with raising Se/Me-ratio [4, 5]. Further the solar cell produced at the lower temperature is strongly (220)/(204)-oriented, whereas the solar cell, produced under higher temperature, is (112)-oriented. From other publications we would expect, that the (220)/(204)-orientation leads to improved solar cells, because the CIGSe orientation can influence the junction between CdS and CIGSe [3, 13, 14]. In comparison with our reference solar cell, the main differences are in the open circuit voltage (V_{OC}) and the short circuit current density (J_{SC}). As anticipated V_{OC} is increased due to the enhanced GGI. But J_{SC} is smaller than anticipated [12].

If we take a look at the solar cell parameters according to the Se/Me-ratio, shown in figure 6, we can see a maximum at Se/Me=5. But the fill factor (FF) at T_1=490°C or V_{OC} at T_1=400°C seems to increase after

passing Se/Me=6 towards higher Selenium pressures. Hence it is necessary to prepare further absorber layers with increased Se/Me-ratio to study the behavior at even higher Selenium overpressure although this may have no technological relevance. The absorber layers which are prepared with Se/Me=2.1 did not show any photovoltaic action probably due to Cu_2Se formation. To investigate the strong reduction of J_{SC} in comparison to the reference cell, we measured the external quantum efficiencies (EQE) (figure 7). The maximum EQE as well as the collection at long wavelengths is strongly reduced, in comparison to the reference. This can be attributed to the increased GGI which leads to a significant reduction at long wavelengths. With regard to the Selenium variation, we can see a similar behavior for both substrate temperatures. From Se/Me=3.9 to 5 the whole EQE is increased, but for higher Se/Me-ratios the EQE decreases. This is in contrast to the literature, where an increased or constant J_{SC} and EQE is shown [5].
In addition we have measured the time dependency of V_{OC}. Therefore the solar cells were relaxed over 16 hours at 40°C in darkness. V_{OC} was measured at constant 25°C under illumination. Independent from the Se/Me flux ratio V_{OC} increases under illumination. This is in disagreement with the findings in reference [7], which shows a decreasing VOC for low Selenium pressures.

4 CONCLUSION

The Se/Me-ratio shows a significant influence on the preferred orientation of the CIGSe layers. It differs from highly (112), for 2.1< Se/Me<4, to (220)/(204)-oriented, for Se/Me>4. On the other hand, crystal size and RAMAN-spectral features are generally independent from the Se/Me ratio. Furthermore we showed a clear maximum for solar cell parameters at Se/Me=5, which differs from other publications.
A main problem, that complicates the comparability to the literature is the high sodium concentration located to the GB inside the absorber layer of our solar cells.

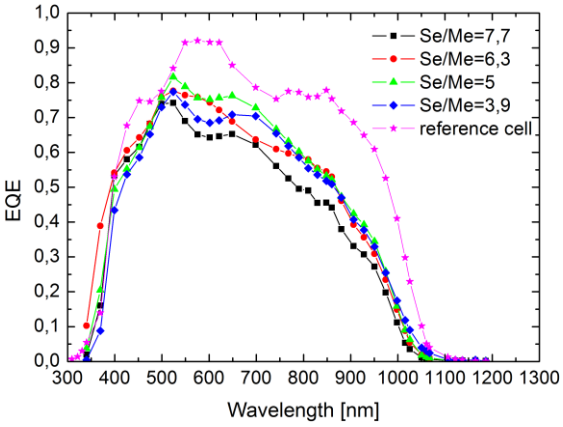

Figure 7: External quantum efficiency measurements for 400°C first stage substrate temperature with respect to the Se/Me-ratio.

5 REFERENCES

[1] KAUFMANN, C.A. ; NEISSER, A. ; KLENK, R. ; SCHEER, R., In: Thin Solid Films 480-481 (2005), S. 515–519
[2] KIM, K. H. ; YOON, K. H. ; YUN, J. H. ; AHN, B. T., In: Electrochemical and Solid-State Letters 9 (2006), S. A382–A385
[3] CHAISITSAK, S. ; YAMADA, A ; KONAGAI, M., In: Jap.J.Appl.Phys. 14 (2002), S. 507–513
[4] HANNA, G. ; MATTHEIS, J. ; LAPTEV, V. ; YAMAMOTO, Y. ; RAU, U. ; SCHOCK, H. W., In: Thin Solid Films 31 (2003), S. 431–432
[5] ISHIZUKA, S. ; YAMADA, A. ; FONS, P. ; N., Shigeru, In: Prog. Photov. (2011). http://dx.doi.org/10.1002/pip.1227
[6] Islam, M.M. , Sakurai , T., Ishizuka, S., Yamada, A., Shibata, H., Sakurai, K., Matsubara, K., Niki, S., Akimoto, K., In: Journal of Crystal Growth 311 (2009) S. 2212–2214
[7] Kempa, H., Rissom, T., Hlawatsch, U., Gaudig, M., Obereigner, F., Kaufmann, C.A., Scheer, R., In: Thin Solid Films 535 (2013), S. 340-342
[8] SAKURAI, K. ; HUNGER, R. ; SCHEER, R. ; KAUFMANN, C.A. ; YAMADA, Y. ; BABA, T. ; KIMURA, Y. ; MATSUBARA, K. ; FONS, P. ; NAKANASHI, H. ; NIKI, S., In: Progress in Photovoltaics 12 (2004), S. 219–234
[9] CONTRERAS, M.A. ; EGAAS, B. ; KING, D. ; SWARTZLANDER, A. ; DULLWEBER, T., In: Thin Solid Films 361-362 (2000), S. 167
[10] RAMANATHAN, K. ; CONTRERAS, M.A. ; PERKINS, C.L. ; ASHER, S. ; HASOON, F.S. ; KEANE, J. ; YOUNG, D. ; ROMERO, M. ; METZGER, W. ; NOUFI, R. ; WARD, J. ; DUDA, A., In: Progress in Photovoltaics 11 (2003), S. 225–230
[11] BRAUNGER, D. ; HARISKOS, D. ; BILGER, G. ; RAU, U. ; SCHOCK, H.W., In: Thin Solid Films 361-362 (2000), S. 161
[12] SCHEER, R. ; SCHOCK, H.-W.: Chalcogenide Photovoltaics. Weinheim : Wiley-VCH, 2011, S. 151 and S.287
[13] CONTRERAS, M. ; EGAAS, B. ; RAMANATHAN, K. ; HILTNER, J. ; HASOON, F. ; NOUFI, R., In: Progress in Photovoltaics: Research and Applications 7 (1999), S. 311–316
[14] YOON, J.-H. ; KIM, W.-M. ; PARK, J.-K. ; BAIK, Y.-J. ; SEONG, T.-Y. ; JEONG, J.-h., In: Prog. Photov. (2012). http://dx.doi.org/10.1002/pip.2338